Available online at www.sciencedirect.com

ScienceDirect

Acta Materialia 61 (2013) 7173–7179

Acta MATERIALIA

www.elsevier.com/locate/actamat

Phase growth in an amorphous Si–Cu system, as shown by a combination of SNMS, XPS, XRD and APT techniques

Bence Parditka [a,b], Mariana Verezhak [a,c], Zoltán Balogh [d,*], Attila Csik [e], Gábor A. Langer [a], Dezső L. Beke [a], Mohammed Ibrahim [d], Guido Schmitz [d], Zoltán Erdélyi [a]

[a] Department of Solid State Physics, University of Debrecen, P.O. Box 2, H-4010 Debrecen, Hungary
[b] Aix-Marseille Université, IM2NP, Faculté des Sciences de Saint-Jérôme case 142, 13397 Marseille, France
[c] Metal Physics Department, National Technical University of Ukraine 'Kyiv Polytechnic Institute', 37 Prospect Peremogy, U-03056 Kiev, Ukraine
[d] Institute of Materials Physiks, University of Münster, Wilhelm Klemm Straße 10, D-48149 Münster, Germany
[e] Institute of Nuclear Research of the Hungarian Academy of Sciences (Atomki), H-4001 Debrecen, P.O. Box 51, Hungary

Received 4 February 2013; received in revised form 9 August 2013; accepted 11 August 2013
Available online 14 September 2013

Abstract

It is shown, by the combination of secondary neutral mass spectrometry (SNMS), X-ray diffraction and atom probe tomography (APT), that the growth of a Cu_3Si crystalline layer between amorphous Si and nanocrystalline Cu thin films at 408 K follows a linear law and the shifts of the Cu_3Si/Cu and Cu_3Si/amorphous Si interfaces contribute approximately equally to the growth of this phase. It is also illustrated that the Si atoms diffuse rapidly into the grain boundaries of the nanocrystalline Cu, leading to Si segregation on the outer surface and to an increase in the overall Si content inside the Cu layer. Both the SNMS and APT results indicate that, even during the deposition of Cu on the amorphous Si, an intermixed region (of about 10 nm thick) is formed at the interface. This readily transforms into a homogeneous Cu_3Si crystalline reaction layer which grows further, apparently following an interface-controlled linear kinetics.

Keywords: Silicide; Solid state reaction; SNMS; APT; XPS

1. Introduction

Thin crystalline silicon (c-Si) films are key materials for low-cost, high-efficiency solar cells [1,2], as the maximum efficiency of amorphous silicon (a-Si) solar cells is still restricted by the structural metastability and disorder of the films. However, physical vapor deposited thin Si films are usually amorphous and the crystallization temperature of Si is very high (~1000 K), which requires expensive, heat-resistant substrates (e.g. quartz glass) and high thermal budgets. The maximum possible temperature for different substrates can be seen, for example, in Fig. 1 of Ref. [3].

Metal-induced crystallization (MIC) offers a way to circumvent this problem as the crystallization temperature of Si in contact with certain metals is drastically reduced [3]. Generally, two different procedures can cause MIC. In the case of low-melting materials like Al [4], metal-induced bond weakening [5] destabilizes the a-Si, hence allowing crystallization at a reduced temperature. Silicide-forming materials such as Ni [6] may follow another route, where the silicide acts as a template for nucleating c-Si. Cu is well known to form multiple silicide phases [7], and previous investigations have shown that MIC process proceeds with the aid of Cu_3Si phase [8,9].

In Li-ion secondary batteries, Si nanowires or nanorods used as anodes possess higher specific capacity and larger surface areas compared to traditional graphite anodes. This results in an increased energy density and faster charg-

* Corresponding author. Tel.: +49 251 83 39016.
E-mail address: zbalo_01@uni-muenster.de (Z. Balogh).

1359-6454/$36.00
http://dx.doi.org/10.1016/j.actamat.2013.08.021

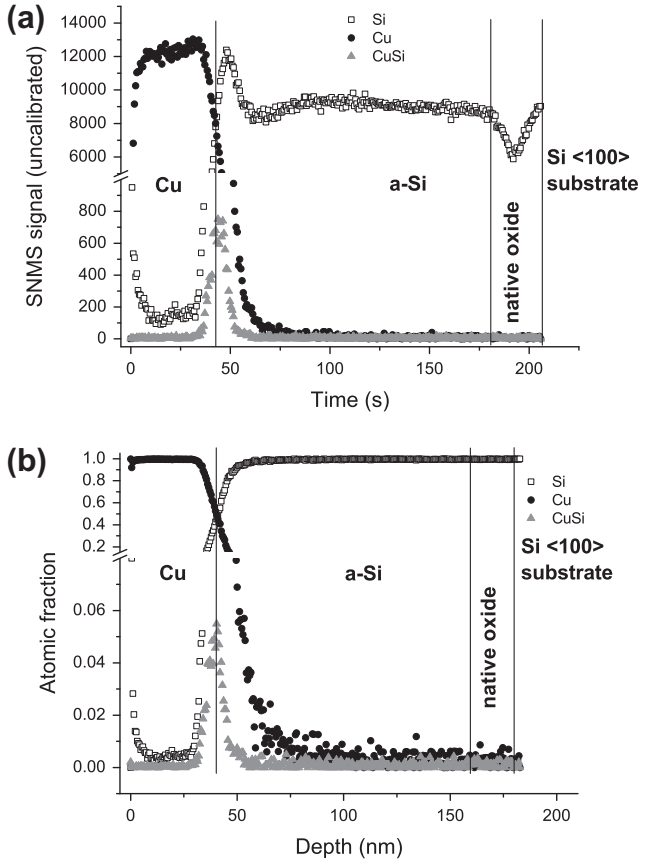

Fig. 1. The raw (intensity vs. time) SNMS depth profile for the deposited sample (45 nm Cu/120 nm a-Si//Si⟨100⟩). Three different mass ranges, belonging to Si (28 amu), Cu (63 amu) and CuSi (28 amu + 63 amu = 91 amu) molecules, were measured. (a) The crossing of the Cu and Si signals marks the position of the interface in the as-deposited sample. The position of the substrate is marked by the reduction of the Si signal due to the presence of the native oxide. The apparent Si peak at the Cu/Si interface is a well-known artifact caused by the change of sputtering conditions at the metal–semiconductor transition. (b) The composition profile determined from (a) (see the text in Section 3 for details). The vertical lines mark the interfaces.

ing–discharging, along with a number of other advantages [10]. On the other hand, there are also some very undesirable properties. The anode arrangement is brittle, due to its fragile structure and the large volume change during the insertion and extraction of lithium ions. Consequently it loses its initial shape and electric properties quickly, which shortens the lifetime of the battery. Previous investigations [11,12] highlighted the possibility of increasing the cyclic stability by complementing the structure with a copper coating or the co-deposition of Si and Cu during the fabrication of the nanorods, which, according to the above-mentioned literature, remarkably increase the reversible capacity and the flexibility of these power sources.

In the case of both MIC and battery electrodes, it has been shown by X-ray photoelectron spectroscopy (XPS) and X-ray diffraction (XRD) that Cu_3Si phase appears during the fabrication process. Studying the formation and the later development of this phase is therefore of technological importance, especially at the low temperatures used in battery-related applications. The Cu_3Si phase starts growing at a very low temperature. Her et al. [9] observed the appearance of this phase between 370 and 520 K. Moreover depositing an a-Si/$Cu_{70}Si_{30}$ layer, Ou et al. [13] reported the formation of crystalline Cu_3Si grains in the as-prepared layer. The kinetics of the phase growth in the 450-500 K range was found to be parabolic by Chromik et al. [14], whereas in some metal/Si systems non-Fickian phase growth kinetics was observed [15–20].

In this article we present a study of the early stages of the Cu_3Si growth by a combination of experimental techniques.

2. Experimental details

Bilayer structures were prepared by direct current magnetron sputtering at ambient temperature. First, a 120 nm of a-Si layer was deposited onto the Si⟨100⟩ substrate, followed by a 45 nm thick Cu layer. The base pressure in the main chamber was 5×10^{-7} mbar. Cu (99.99%) and Si (99.999%) targets were applied as sputtering sources. The sputtering was performed under the dynamic flow of Ar (99.999%) at a pressure of 5×10^{-3} mbar and the sputtering power was 40 W for each specimen and target. All specimens were cut into half. One part was kept as prepared, while the other could be annealed. The sizes of the samples were much smaller than the homogeneous zone of the magnetron sources. Accordingly, a good homogeneity of the layer thickness and structure can be expected across the whole of the specimen surface. The sputtering rates were calibrated from the thickness of the previously sputtered layers using an AMBIOS XP-1 profilometer.

The thickness of the layers in the as-prepared samples was determined for all bilayer specimens by a combined method [20]. First, a secondary neutral mass spectrometry (SNMS) depth profile was taken for each sample until the substrate was reached. This transition is marked by a decrement of the Si (28 amu) signal due to the presence of the native oxide (Fig. 1a). A second crater was then bored to the depth where the Si and Cu (63 amu) signals became equal. The depth of these craters was measured by the profilometer. The depth of the second crater gave the thickness of the Cu layer (41.6 ± 1.6 nm, the error representing the standard deviation of 21 individual crater depths) and was set as the position of the original Cu/Si interface. Systematic errors stemming from the criterion used to determine the interface position cannot exceed a few nanometers since the Cu/Si transition zone was found to be adequately narrow, in the range of 10 nm (Fig. 1).

In order to determine the annealing temperature and time, we performed resistivity measurements on specimens deposited over single crystalline Al_2O_3⟨111⟩ substrates. Sapphire was selected since it is an insulating material. XRD patterns were taken from these samples both before

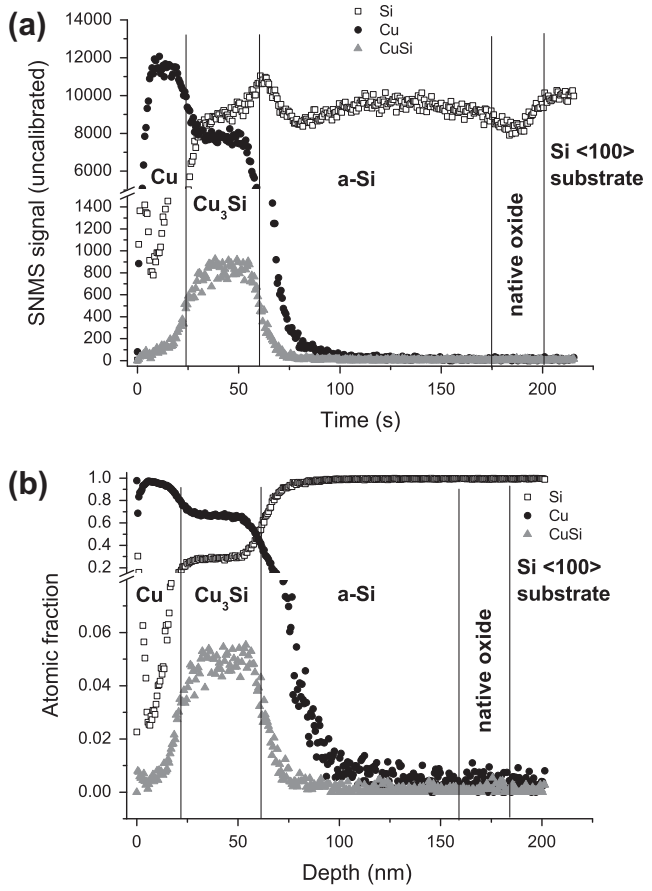

Fig. 2. SNMS profile of a sample annealed at 408 K for 12 h. (a) Raw intensity vs. time data. (b) A conversion to the more convenient atomic fraction vs. depth representation. The presence of the intermetallic phase is clearly indicated by a nearly flat region on the Cu and Si curves. The molecular CuSi curve also possesses a plateau in the same region. Vertical lines indicate the interfaces between the main phases in the specimen.

and after the annealing treatments to identify the (crystalline) phases present in the samples.

On the basis of these test measurements, the following heat treatments were performed: 1, 2, 4, 8, 12 and 18 h at 408 K (under a high vacuum of $\sim 10^{-6}$ mbar). In order to mimic the heating up and cooling down effects, we also applied a "t_0" annealing treatment, i.e. we heated specimens up to 408 K and then immediately let them cool down.

In order to determine the position of the formed phase boundaries after annealing, the heat-treated samples were also analyzed by SNMS. As well as the mass ranges of the Si and Cu, we also followed the CuSi (28 + 63 amu) molecules during the depth profiling. The detected molecular CuSi originates from either sputtered CuSi molecules or molecules formed by a later recombination of separately sputtered Cu and Si atoms (Fig. 2). Irrespective of the origin, however, these molecules are good indicators that both copper and silicon were present in the desorbed layer. In order to determine the top and bottom positions of the growing intermetallic phase, the ion bombardment was stopped at the point where the CuSi intensity curve dropped to half of the plateau value in the reaction layer. The depth of the craters was determined after each individual SNMS measurement by the profilometer, just as in the case of the as-prepared samples. Because of the destructive nature of the SNMS analysis, separate specimens were required for each analysis.

To reveal information concerning the interface chemistry, we compared the XPS spectra recorded at the interface of the as-deposited samples to those recorded at the product layer in the annealed counterpart samples. XPS measurements were performed with a PHOIBOS HSA3500 100 R6 X-ray photoelectron spectrometer.

To gain three-dimensional information on the initial reaction process, an atom probe study was carried out using a laser-assisted tomographic atom probe unit [21]. This instrument has a delay line detector system with 120 mm diameter and an aperture angle of 30°. Optimal measurement conditions were achieved using an ultraviolet (340 nm wavelength) laser, with 220 fs pulse length, ~0.1 μJ pulse energy and 200 kHz repetition rate. For these investigations, a layer system of 20 nm Cu/40 nm a-Si was deposited onto field-developed tungsten tips (W). The samples were annealed in ultrahigh vacuum conditions ($p < 10^{-7}$ mbar).

3. Results

3.1. Structure characterization and phase identification

Figs. 1 and 2 show SNMS depth profiles for the as-prepared and the corresponding annealed samples (408 K, 12 h), while Fig. 3 shows the broadening of the region from which CuSi molecules are detected. The depth scale was determined on the basis of profilometer measurements. First, we measured the position of each main interface (marked by vertical lines), then, as the intensities vary only

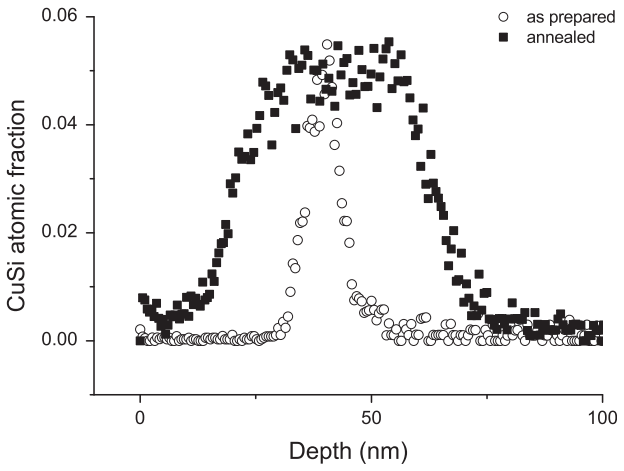

Fig. 3. Atomic fraction of the molecular CuSi vs. depth in an as-prepared and an annealed (408 K, 12 h) specimen. A plateau can be seen in the case of the annealed sample, which indicates that the Cu_3Si product phase is characterized by minor composition variations.

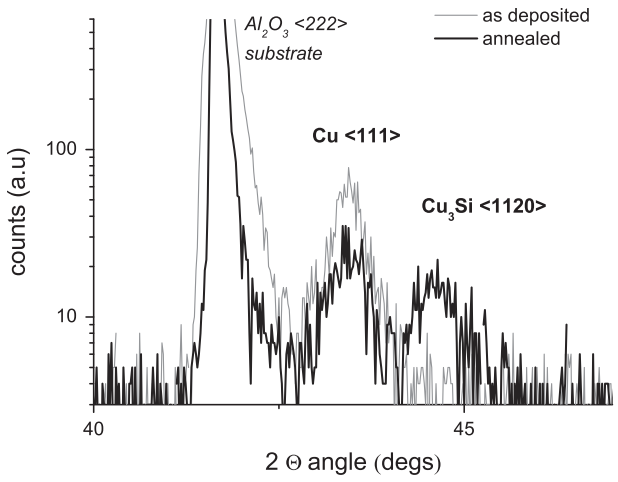

Fig. 4. X-ray diffractograms on Cu/a-Si films deposited on sapphire ⟨1 1 1⟩ substrates. The gray curve corresponds to the as-deposited sample, the black one to the annealed sample (at 408 K for 18 h). In the as-deposited specimen only reflections belong to metallic Cu can be observed; the ⟨1 1 2 0⟩ peak of Cu_3Si appears after the annealing treatment.

slightly, we assumed a constant sputtering rate between these fix points and calculated the depth scale from the sputtering time.

To determine the relation between the measured intensities and the real concentration, one needs to know the isotope abundance and the detection efficiency. Since the latter is composition dependent, reference samples from a wide range of concentrations are required for an exact calibration procedure. As can be seen from the raw curves of Fig. 1a and Fig. 2a, the Cu and a-Si zones are practically free of impurities, thus any actual detection efficiency corresponds to that of the pure Cu or Si. Moreover, the interfaces are quite abrupt and the Si and Cu intensity

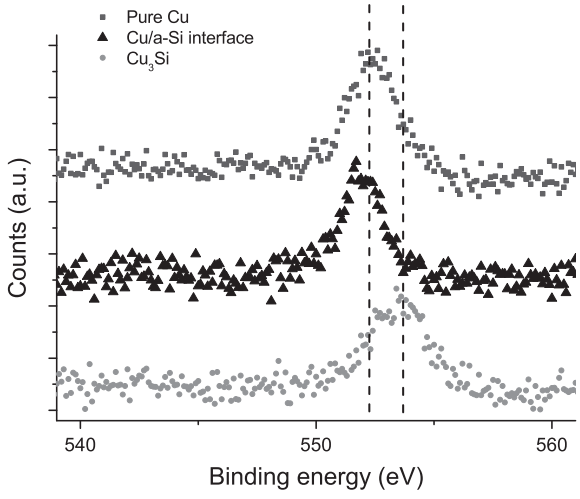

Fig. 5. XPS spectra (showing only the range of interest) obtained in the pure Cu layer (dark gray squares) and at the interface region (black triangles) in an as-deposited sample, and in the Cu_3Si phase of its annealed counterpart (gray circles). The two dashed lines indicate the maximum of the Cu 2*p* peak for the Cu and the Cu_3Si phase. The interface region clearly shows a chemistry more similar to the metallic Cu than to Cu_3Si.

curves in the silicide phase are reasonably flat. Therefore we only have to adjust the parameters for this phase. From the XRD measurements (see below), we know that the growing phase is Cu_3Si; thus, the SNMS depth profile should show the presence of this phase. This means that the ratio of the Si and Cu composition must be adjusted to 1:3, according to the formula Cu_3Si. To check the validity of the parameters, we observed the behavior of the CuSi molecular species. This molecule requires the presence of both Cu and Si, and should show a maximum when the Cu and Si compositions are identical. As can be seen in Figs. 1 and 2, these assumptions indeed give self-consistent results.

The Cu/Si transition zone is about 10 nm wide in the case of the as-prepared state. This shows that, even considering technique-related effects, the Cu and Si atoms at the interface intermixed during preparation. On the other hand, the intensity and composition curves are smooth at the interface, i.e. we found no trace of a Cu_3Si layer, unlike Ou et al. [13]. This is also supported by our XRD, XPS and APT measurements, as can be seen below.

Fig. 4 shows the results of the XRD measurements performed on the as-deposited sample and the annealed sample in order to reveal if a detectable Cu_xSi_y phase exists at the interface before heat treatment and to determine which phase evolves during the heat treatment. In the case of the annealed sample (18 h long heat treatment at 408 K), one can see the ⟨1 1 2 0⟩ peak of the newly grown hexagonal Cu_3Si phase. The same peak could not be observed for the as-prepared state, indicating that there was only a very small amount of Cu_3Si present, if any.

Fig. 5 shows XPS spectra recorded in the pure Cu layer, at the Cu/a-Si interfaces for the as-received sample and inside the Cu_3Si phase for the annealed counterpart sample. As can be seen, in the case of the annealed sample, the position of the peak corresponding to the Cu 2*p* photoelectrons is shifted compared to that in the pure Cu layer. However, this shift is not present in the case of the as-deposited sample. This indicates that the Cu_3Si phase did not exist before heat treatment, and that the examined phase formed by the annealing process.

3.2. Phase growth

In order to investigate the kinetics of the shift of the interfaces and the growth rate of the Cu_3Si phase, an integral form of the linear parabolic growth [19,22–24],

$$\frac{x^2}{2D} + \frac{x}{K} = t - t_0 \tag{1}$$

can be used, where x, t and t_0 are the thickness, the time and an integration constant, respectively. D and K, apart from a constant factor in the order of unity [24], are the interdiffusion coefficient (assumed to be composition independent) in the phase and an effective interface rate coefficient ($K^{-1} = K_1^{-1} + K_2^{-1}$, where K_1 and K_2 belong to the interfaces bordering the phase [24]), respectively. When Eq. (1) is

applied for the shift of an individual interface, K is obviously the interface rate coefficient of this interface [25].

Fig. 6 shows the interface shifts as a function of annealing time obtained by a combination of SNMS and profilometer measurements, as discussed in Section 2. In each case, the depths of the produced craters were measured by the profilometer several times and in several directions to obtain an accurate averaged depth value. In these plots the origin corresponds to the position of the interfaces obtained after the t_0 annealing. Interestingly, we observed the formation of a definite thick (about 20 nm thick) Cu_3Si layer after this t_0 annealing (see also below), and we always show the growth kinetics after this "formation" period in the kinetic plots (Figs. 6 and 7).

The 1:3 stoichiometry of Si to Cu should result in a significantly higher Cu consumption, even with the density differences taken into account, though, interestingly, there is no real difference between the consumptions of Si and Cu, or even a slightly greater loss of Si. A possible explanation for this phenomenon could be the diffusion of Si into the Cu grain boundaries, which would cause an overall shrinkage of the Si layer and the growth of the Cu layer. As can be seen in Fig. 2, Si shows a small segregation peak near the surface and an easily measurable average Si composition throughout the whole Cu layer. The Cu composition, in contrast, falls to zero upon reaching the Si layer. This clearly shows that the solid-state reaction is accompanied by significant Si grain boundary diffusion into the Cu layer. APT measurements carried out at somewhat higher temperatures (438 K) support this picture (see Fig. 8).

According to Fig. 6, the shift rates of the two interfaces are very similar (almost the same curve can be fitted to both curves within the experimental errors), indicating that

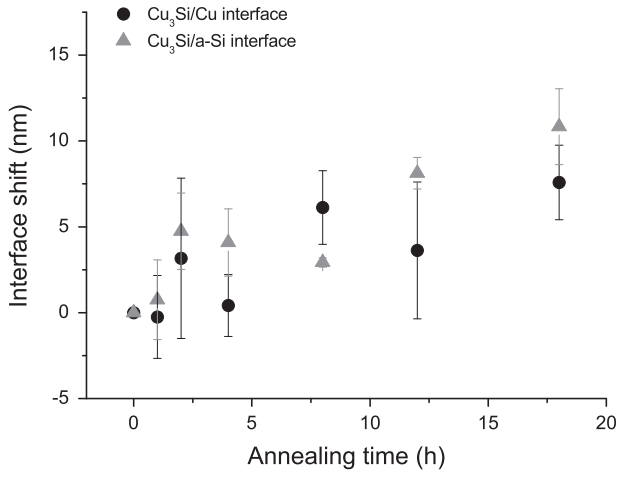

Fig. 6. Distance of Cu_3Si phase boundaries (interfaces) measured from the position of the interfaces after the t_0 annealing (see the text). Cu/Cu_3Si interface denotes the interface between Cu and Cu_3Si, whereas Cu_3Si/a-Si denotes the interface between the Cu_3Si and a-Si. The data points represent average values of three successive independent measurements. Despite the 1:3 stoichiometry, the consumption of the two materials (surprisingly) shows no clear difference.

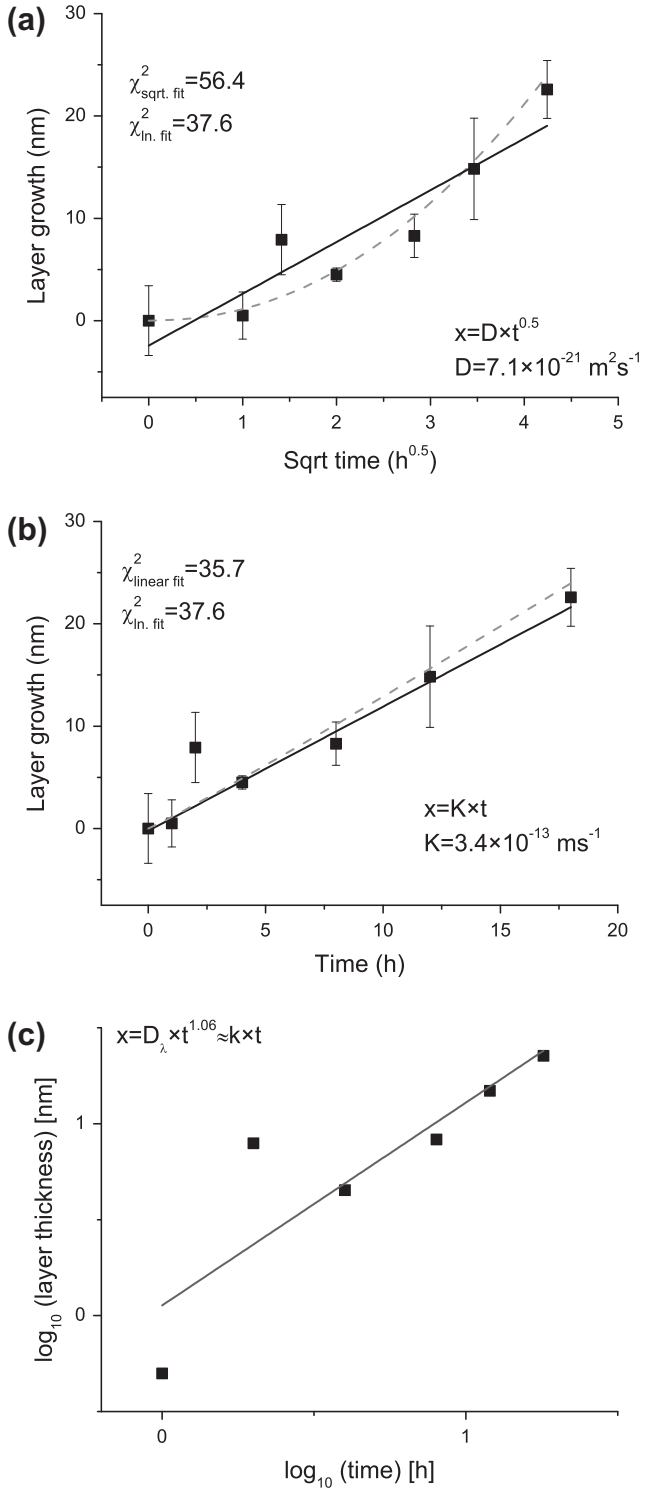

Fig. 7. Evolution of the total thickness of the Cu_3Si layer in different representations: (a) as a function of the square root of time, (b) as a function of time (linear scale) and (c) as a double logarithmic representation. The solid black lines represent the straight line fitted to the data in the given representation. Parabolic growth is clearly the worst estimate of the measured data, while the linear growth assumption and the log–log fitting provide comparable results. For convenience, the power function (generalized power law of diffusion/reaction – see the text) obtained from the fitting on the log–log scale is also plotted by dashed gray curves in (a) and (b). The χ^2 values of the different fittings are also shown.

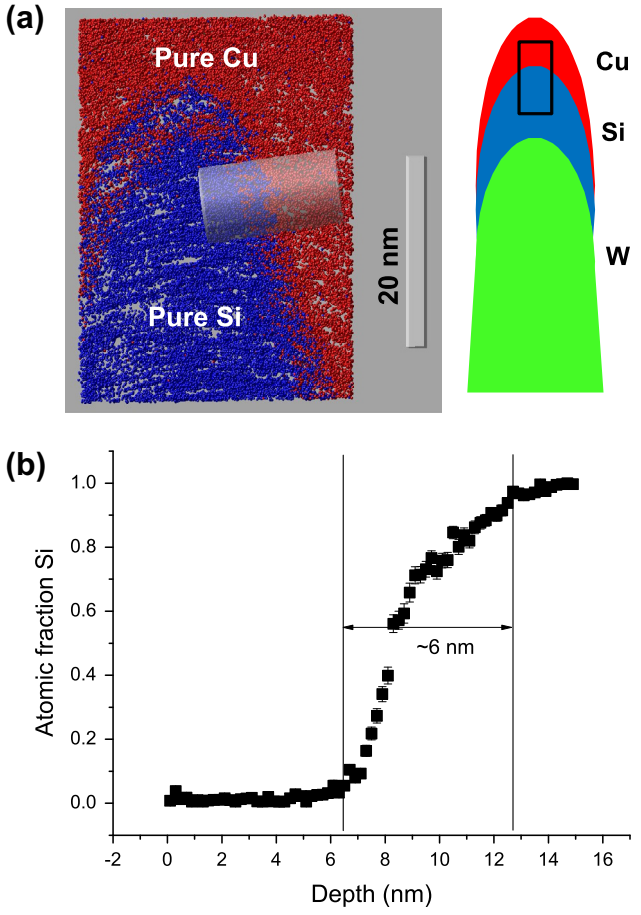

Fig. 8. (a) Part of the reconstructed measurement from an as-prepared specimen (Cu atoms are represented by red/lighter balls, Si atoms by blue/darker balls). A relatively broad mixed zone is visible at the interface. The sketch of the geometry and the position of the section in the specimen can be seen on the right-hand side. (b) Si composition profile within the analysis cylinder. Some inhomogeneity appears on the nanoscale; however, we found no trace of the Cu_3Si phase in the as-prepared state. Error bars represent the sampling error of the sections. (For interpretation of the references to color in this figure legend, the reader is referred to the web version of this article.)

the effective parameters determining the shift have similar values. (The attribute "effective" is used to indicate that at least two types of atomic jumps – grain boundary and bulk – are involved). Nevertheless, using a linear fit, one obtains $K_1 \cong K_2 = (1.5 \pm 0.5) \times 10^{-13}$ ms^{-1}.

Since, in the literature, the growth of the reaction layer is usually analyzed, it was worth repeating this for the growth of the Cu_3Si phase. In Fig. 7 the thickness of the Cu_3Si phase is plotted against the square root of the annealing time (Fig. 7a), against the annealing time (Fig. 7b) and on a double logarithmic scale (Fig. 7c). Even a crude comparison reveals that the assumption of a linear growth rate offers a much better description than the standard parabolic model. The χ^2 value of the former model is less than two-thirds that of the latter (35.7 and 56.4, respectively). Since all fitting functions contain the same number of free parameters, a direct comparison of these values is possible. We can therefore conclude that we observed an anomalous linear growth process that lies in the so-called superdiffusive regime [26]. Our results may thus also contribute to the understanding of anomalous growth processes in solids as well as their importance in other fields (metal–silicon contact [27], metal-induced recrystallization). From the fitting with the linear term in Eq. (1), linear growth (see Fig. 7b and c) with a reaction rate coefficient of $K = (3.4 \pm 0.4) \times 10^{-13}$ ms^{-1} can be deduced at 408 K. As expected, the Cu_3Si/Cu and Cu_3Si/a-Si interfaces contribute equally to the growth and thus $K \cong 2K_1$ (or $2K_2$) within the error bars. This value of K can be compared to the K value calculated from the Arrhenius function of the interface reaction rate coefficient given in Ref. [19] for the growth of Ni_2Si phase on an Si wafer. This leads, at 408 K, to a coefficient of the same order of magnitude: $K = 3.25 \times 10^{-13}$ ms^{-1}.

Let us now turn back to the rapid formation of the Cu_3Si phase during t_0 annealing. This suggests that some precursor intermixed layer should exist between the Cu and Si, even in the as-deposited case. This is also supported by the relatively wide 10 nm thick transition zone between the Cu and Si in the SNMS depth profiles.

Fig. 8a shows a section from an atom probe reconstruction of a layer stack in the as-deposited state. A mixed region containing both Cu and Si atoms is clearly observed. Analysis cylinders were placed across the mixed zone perpendicular to the interfaces (perpendicular to isoconcentration contours) to determine the local concentration profiles. Fig. 8b presents such a composition profile (the cylinder diameter was 4 nm, the section length was 0.2 nm and no moving average was used to smoothen the data). This (local) composition profile demonstrates a relatively broad (5–10 nm) transition that was more or less smooth; the apparent Si and Cu richer domains visible in Fig. 8a are already washed out. This is especially true for the macroscopic lateral sizes analyzed by SNMS in Fig. 1.

Two distinct stages in solid-state reaction to the Cu_3Si phase clearly appear, initialized by the mixed layer formed at deposition. First a very rapid process creates an ~20 nm thick intermetallic layer; indeed, this layer is already present after the "t_0" annealing. This is followed by a very sluggish growth, which proceeds linearly in time and duplicates this initial width only after ~18 h at 408 K. Here, we focused quantitatively on the second stage, always subtracting the thick, dense initial Cu_3Si layer. The details of the initial phase formation are nevertheless an interesting research topic on their own, and will be analyzed in a separate study.

Fig. 9 shows a section of ATP measurement after annealing (at 438 K for 5 h). In addition to the Si segregation to the free surface and the increase in the overall Si content inside the Cu layer – in line with the SNMS results – another Si segregation zone appears at the Cu/Cu_3Si interface. The presence of such a layer is not visible in the SNMS measurement, even though it is quite prominent in the APT map.

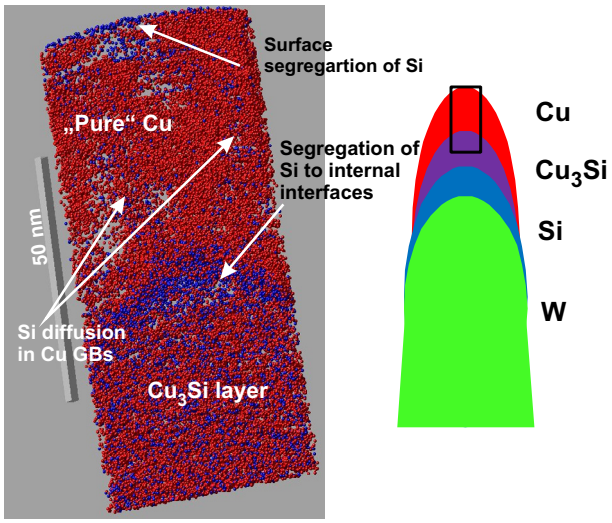

Fig. 9. Section of an APT measurement after annealing the specimen for 5 h at 438 K. A well-developed silicide layer is visible at the bottom. (The color coding is the same as in Fig. 8.) Si segregation to the free surface and at the Cu/Cu_3Si interface appears, as well as Si-rich stripes in the Cu (most probably grain boundaries). A sketch of the measurement geometry is shown on the right. (For interpretation of the references to color in this figure legend, the reader is referred to the web version of this article.)

The distribution of the Si atoms in the Cu layer is not homogeneous: there are stripes of higher concentrations of Si atoms, with zones of pure Cu in between. A more careful analysis, using multiple sections from different directions, revealed that these zones are interconnected, thus this is a result of the Si diffusion in the Cu grain boundaries. Accordingly, the main features of the SNMS intensity curves are well supported by direct local analysis.

4. Conclusions

In this paper we present a study of the growth of Cu_3Si by the combined application of complementary experimental techniques: SNMS, XPS, XRD and APT. We show that the Cu_3Si is formed at the interface during annealing, but does not exist in the as-deposited samples. Interestingly, the growth of the Cu_3Si phase is found to be anomalous, i.e. the thickness of the growing phase increases proportionally with time (superdiffusion). Furthermore, it is demonstrated that the shifts of the Cu_3Si/Cu and Cu_3Si/a-Si interfaces contribute to the growth of the phase approximately equally.

The correct interpretation of this anomalous growth kinetics needs further investigations to determine whether it is a consequence of the reaction control or the high diffusion asymmetry of the components, which can also lead to anomalous (different from parabolic) growth kinetics [22,23].

Furthermore, the sudden formation of a relatively thick crystalline Cu_3Si layer is observed just after a heating up and cooling down (with the maximum temperature of the later isotherm treatments). APT analysis showed that precursors of intermixed regions (between the as-deposited Cu and Si) are already present immediately after the deposition, and these probably can be easily transformed into a homogeneous crystalline, rather thick Cu_3Si layer in the very early stage of aging.

Cu_3Si is a possible initiator of metal-induced crystallization and can play a role in Si-based Li-ion batteries. Kinetic data, especially low-temperature kinetic data, of such battery applications is therefore of great importance. Based on the linear growth relation, we found a reaction rate of $3.4 \pm 0.4 \times 10^{-13}\,\mathrm{m\,s^{-1}}$, or roughly $1\,\mathrm{nm\,h^{-1}}$, at 408 K.

Acknowledgements

This work was supported by the OTKA Board of Hungary (No. NF101329), by the TAMOP 4.2.2.A-11/1/KONV-2012-0036 and TÁMOP-4.2.2/B-10/1-2010-0024 projects (implemented through the New Hungary Development Plan co-financed by the European Social Fund, and the European Regional Development Fund). M.V. is a grantee of the Visegrad Fund scholarship.

References

[1] Shah A, Torres P, Tscharner R, Wyrsch N, Keppner H. Science 1999;285:692.
[2] Schopp REI, Carius R, Beaucarne G. MRS Bull 2007;32:219.
[3] Wang Z, Jeurgens LH, Wang JY, Mittemeier EJ. Adv Eng Mater 2009;11:131.
[4] Konno TJ, Sinclair R. Philos Mag 1992;66:749.
[5] Hiraki A. Surf Sci Rep 1984;3:357.
[6] Guliants EA, Anderson WA. J Appl Phys 2001;89:4648.
[7] Massalski TB, editor. Binary alloys phase diagrams. Materials Park, OH: ASM International; 1992.
[8] Lee SB, Choi DK, Phillipp F, Jeon KS, Kim CK. Appl Phys Lett 2006;88:083117.
[9] Her YC, Chen CW, Wu CL. J Appl Phys 2006;99:113512.
[10] Chen HX, Dong ZX, Fu YP, Yang Y. J Solid State Electrochem 2010;14:1829.
[11] Chen H, Xiao Y, Wang L, Yang Y. J Power Sources 2011;196:6657.
[12] Au M, He Y, Zhao Y, Ghassemi H, Yassar RS, Garcia-Diaz B, et al. J Power Sources 2011;196:9640.
[13] Ou SL, Kuo PC, Shen SC, Tsai TL, Yeh CY, Chang HF, et al. Appl Phys Lett 2011;99:121908.
[14] Chromik RR, Neils WK, Cotts EJ. J Appl Phys 1999;86:4273.
[15] d'Heurle FM, Gas P. J Mater Res 1986;1:205.
[16] Schlesinger TE, Cammarata RC. Appl Phys Lett 1991;59:441.
[17] Cserháti C, Balogh Z, Csik A, Langer GA, Erdélyi Z, Glodán Gy, et al. J Appl Phys 2008;104:024311.
[18] Cheng JY, Chen LJ. J Appl Phys 1991;69:2161.
[19] Nemouchi F, Mangelinck D, Bergmann C, Gas P, Smith U. Appl Phys Lett 2005;86:041903.
[20] Lakatos A, Langer GA, Csik A, Cserhati C, Kis-Varga M, Daroczi L, et al. Appl Phys Lett 2010;97:233103.
[21] Schlesiger R, Oberdorfer C, Würz R, Greiwe G, Stender P, Artmeier M, et al. Rev Sci Instrum 2010;81:043703.
[22] Deal BE, Groves A. J Appl Phys 1995;36:3770.
[23] Philibert J. Mat Sci Forum 1994;155–156:15.
[24] Gössele U, Tu K. J Appl Phys 1982;53:3252.
[25] Beke DL, Erdélyi Z, Balogh Z, Cserháti Cs, Katona GL. J Nano Res 2009;7:43.
[26] Klafter J, Sokolov I. Phys World 2005;18:29.
[27] Erdélyi Z, Beke DL. J Mater Sci 2011;46:6465.